No-Reference Noise and Blur Detection via the Fourier Transform

Richard W. Dosselmann and Xue Dong Yang

Technical Report CS-2012-01
August 2012

Department of Computer Science
University of Regina
Regina, SK, CANADA
S4S 0A2

ISSN 0828-3494
ISBN 978-0-7731-0714-4 (on-line)

No-Reference Noise and Blur Detection via the Fourier Transform

Richard Dosselmann and Xue Dong Yang
Department of Computer Science, University of Regina
3737 Wascana Parkway, Regina, Saskatchewan, Canada S4S 0A2
{dosselmr, yang}@cs.uregina.ca

Abstract

This research presents a new method of distinguishing between noisy, blurred and otherwise uncorrupted images via the Fourier transform. The spectrum of an image corrupted by noise is markedly different from one that is marred by blurring, or one that is not damaged at all. In particular, there are more high frequency terms in the spectrum of a noisy image than in that of a blurred image, and, to a lesser degree, that of an image that has not been altered. So as to better emphasize these distinctions, a cumulative distribution function of the terms of the spectrum of an image is assembled. Using only this construct, a new technique that enables a machine to reliably assess the number of high frequency terms in an image, and therefore differentiate among the three types of images, is brought forward.

Keywords: noise, blur, Fourier transform, cumulative distribution function, image quality metric

1 Introduction

Images [1] are frequently disrupted by *noise* [2]. This distortion may turn up as part of the initial acquisition stage, or later, perhaps during transmission. Among the most common types of noise are the *uniform* [1], or, in this work, *random*, *Gaussian* [1] and *salt-and-pepper* [1] varieties. *Blurring* [3] is another troublesome issue. Failing to properly focus a camera, for example, may bring about this error. Most prominent are those stemming from *averaging filters* [1], or, here, an *averaging* blur, as well as *Gaussian* [2] and *motion* [1] blurs. The goal of this research is to automatically identify those images that are noisy or blurred, as well as those in which neither error occurs. The strategy proposed by this research is based on the classic *Fourier transform* [1] (FT) and the realization that a noisy image, transformed to the *frequency domain* [1], contains far more high *frequency* [4] terms than does a blurred image. The primary applications of this work are in the area of *image quality* [2] assessment. Existing image quality *metrics* [5] generally work by comparing an image with its "original" or "perfect" form. The routine absence of an original image greatly limits the utility of these *full-reference* [6] (FR) metrics. While the technique presented in this work is also tested in an FR framework, it is principally designed

to be a *no-reference* [6] (NR) metric, meaning that it functions without any original image. It is therefore ideally suited for real-world applications, such as monitoring television and video content or spotting problems in images taken with a camera or cell phone. Before proceeding, note that the ideas outlined in this work were originally documented in [7, 8].

Traditionally, noise has been caught by comparing pixels in local image patches against some preset threshold. Those exceeding this threshold are surmised to be noise. Approaches in this direction include those of [9, 10, 11]. This task is usually easier when more than one image is available, perhaps a sequence of video frames. In this context, any pixel that does not reappear in the frame following the current is deemed to be noise. This is the methodology employed in [12], working specifically with a series of x-rays images. Smolka [13], drawing on the ideas of others [14], measures distances between pixels in a multidimensional space. Complementing these various methods are several based on techniques of *machine learning* [15]. Saradhadevi and Sundaram [16], as an example, train a *neural network* [17] to spot potential noise pixels. In another instance, Zhang and Wang [18] distinguish between pixels belonging to an image and those that are likely noise using *fuzzy logic* [19]. Blurring pares down and warps *edges* [1]. The logical response is therefore to examine the strength of the edges in an image, just as is done in [20, 21, 22], for instance. In a related technique, Levin [23] unearths blurred regions of an image by examining *histograms* [24] of edges. Following a strategy independent of that given in this work, Tolhurst et al. [25] explore the general makeup of images from the perspective of the frequency domain. Liu, Li and Jia [26] also travel down this path, this time looking at the *power spectrum* [1] of an image. Machine learning resurfaces in [27], this time in the form of *support vector machines* [28] (SVM). Here, the authors train their system to recognize the histograms of blurred images, an idea similar in spirit to that of Levin [23].

Following an overview of the new technique in Section 2, the ideas introduced in this work are thoroughly tested in Section 3. Some concluding remarks are then given in Section 4.

2 Method

The intuition behind the method described in this paper is most easily explained by way of an example. Take, then, the scenario depicted in Figure 1. An original image, along with its noisy and blurred counterparts, are given in Figures 1a, 1d and 1g, respectively. The corresponding Fourier *spectra* [1] of these three images are shown in Figures 1b, 1e and 1h, respectively. To allow for improved viewing, all three spectra have been scaled and brightened. The remaining illustrations, namely those of Figures 1c, 1f and 1i, are discussed at length in a moment. One will notice that the outer expanses of the spectrum of Figure 1b are fainter than those of the noisy image, seen in Figure 1e, while it is more cluttered than the spectrum of the blurred picture, given in Figure 1h. The random noise of Figure 1d produces sudden and steep changes in shading values across that image, leading to this increased concentration of high frequency terms in the outer regions of the spectrum of Figure 1e. In an opposite fashion, the averaging blur of Figure 1g smoothes image content, resulting in fewer high frequency terms, just as is observed in Figure 1h. The last case, namely the spectrum of Figure 1b, lies somewhere "in between" these two. The number of high frequency terms in the outer portions of a spectrum is the main focus of this research.

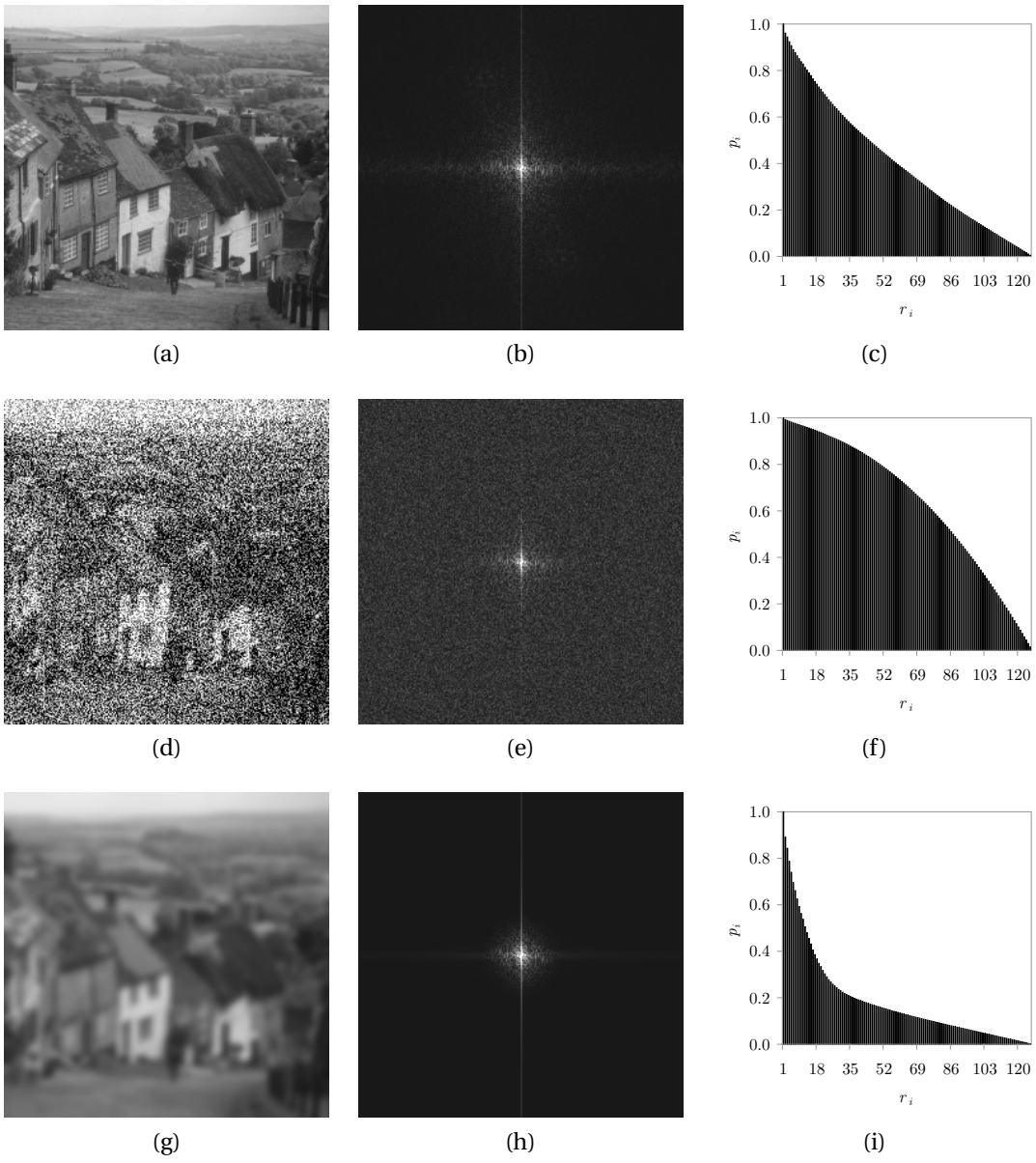

Figure 1: Distinguishing among noisy, blurred and error-free images; (a) “Goldhill”; (b) “Goldhill” spectrum; (c) “Goldhill” CDF; (d) “Goldhill” (57.64% Gaussian noise); (e) “Goldhill” (57.64% Gaussian noise) spectrum; (f) “Goldhill” (57.64% Gaussian noise) CDF; (g) “Goldhill” (11×11 Gaussian blur); (h) “Goldhill” (11×11 Gaussian blur) spectrum; (i) “Goldhill” (11×11 Gaussian blur) CDF

2.1 Cumulative Distribution Function

The first step in the noise and blur detection process is one of gauging the number of high frequency terms in a given spectrum. In this research, a *cumulative distribution function* [1] (CDF) of the values of a spectrum is the tool of choice. Beginning at the outer boundaries of a spectrum, a series of concentric circles, or rings, is superimposed over a spectrum, as depicted in Figure 2. In order for this approach to work, the origin of the spectrum must be moved to the center of that spectrum, the process of which is described in [1]. Suppose now that there are n such rings in total. The outermost ring is computed first. It is denoted r_n. Meanwhile, the innermost, identified as r_1, is calculated last. At this time, the extreme four corners of a

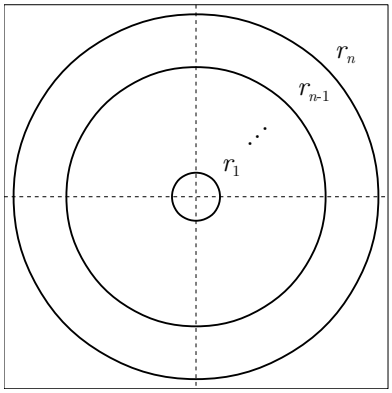

Figure 2: Concentric rings superimposed over a spectrum

spectrum are omitted. Experimental evidence suggests that this corner information is of little value. Moving on, individual sums s_i of the *magnitudes* [1] of the Fourier coefficients of each ring r_i are calculated, where $1 \leq i \leq n$. Let c_i denote next the *cumulative* [29] sum of the terms of the first i rings, that is

$$c_i = \sum_{j=1}^{n-(i-1)} s_{n-(j-1)}. \tag{1}$$

Then, for each ring r_i, the ratio, or proportion, of its cumulative sum c_i to the total sum c_n of all n rings, is computed. Formally, this is given as

$$p_i = \frac{c_i}{c_n}. \tag{2}$$

A normalized value, $0 \leq p_i \leq 1$. Collectively, the p_i terms make up a CDF of the values of a spectrum.

2.2 Noise and Blur Detection

Returning briefly to the example of Figure 1, consider the three CDFs of Figures 1c, 1f and 1i. There is a pronounced "hump" in the center of the CDF of Figure 1f. As the terms in the rings of the outer expanses of the spectrum of Figure 1e are summed, large s_i values in these outlying areas resulting from the noise of Figure 1d rapidly inflate the running total c_i, leading to this "hump" shape. By comparison, there is a "dip" in the CDF of Figure 1i. The mostly bare regions

at the ends of the spectrum of Figure 1h, a consequence of the blur of Figure 1g, initially hold down the value of c_i, giving rise to a CDF that is depressed on the right side. The more or less "balanced" spectrum of Figure 1b yields a progressively increasing series of values, as is apparent from Figure 1c. This last CDF lies "in between" those of the noisy and blurred images. In some sense, images exist along a continuum, with those that are noisy or blurred positioned at opposite ends and the originals centered in between.

The last major step is one of measuring the size of any "hump" or "dip" in a CDF, that is, to decide between noise and blurring, as well as to recognize those images in which neither occurs. To start with, let L be the diagonal line stretching between the tops of the first and last terms, namely p_1 and p_n, respectively, of a given CDF. This is illustrated in the diagram of Figure 3. Here, the terms p_2 and p_3 reach above L, while p_{n-1} and p_{n-2} fall below L. The matching point on L directly above or below a term p_i is denoted L_i. In the example of Figure 3, the points L_3 and L_{n-2}, corresponding to the terms p_3 and p_{n-2}, respectively, are shown. The distance between each pair of values p_i and L_i is written as d_i. Formally,

$$d_i = p_i - L_i. \tag{3}$$

This too is illustrated in Figure 3. Note that in this diagram, $d_3 > 0$, whereas $d_{n-2} < 0$. As a rule,

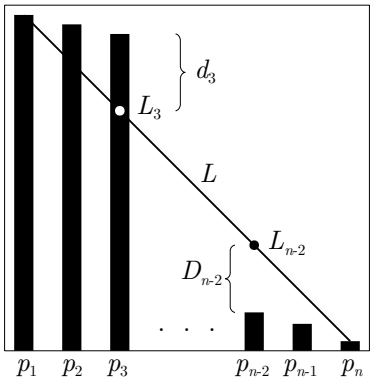

Figure 3: CDF entries p_i above and below L

positive values of d_i suggest a noisy image, while those that are less than zero hint at one that is blurred. Deciding between the two errors is as easy as summing the d_i terms across a CDF. One must be careful, however, as this sum is proportional to the size of the image under investigation. A very large image, having a sizeable CDF made up of many d_i terms, will generally give rise to a large positive, or negative, sum. At the same time, a tiny image, in which there are far fewer d_i terms, produces a much smaller sum. Any sum of the d_i terms must therefore be normalized. Accordingly, this sum is divided by the sum of the n individual L_i terms. It is this adjusted sum, identified as the metric ϕ, that enables a machine to separate noisy, blurred and otherwise uncorrupted images. It is mathematically expressed as

$$\phi = \frac{\sum_{i=1}^{n} d_i}{\sum_{i=1}^{n} L_i}. \tag{4}$$

Typically, ϕ takes on positive values for noisy images and negative values for blurred images. In this work, any image in which ϕ exceeds an experimental threshold of $T_\eta = 0.05$ is said to be

"noisy". "Blurring" occurs whenever $\phi < T_\beta = -0.35$. Lastly, an image is said to be "error-free" whenever $T_\beta \leq \phi \leq T_\eta$.

As mentioned in the opening of Section 1, this metric can also be adapted to operate in a full-reference environment in which there is an original image that can be used as part of a comparison process. In this FR setting, the d_i terms of a noisy image are normally larger than those of the original image. Similarly, these terms are smaller than those of the original in the case of a blurred image. In response, ϕ is redefined for this full-reference case as

$$\phi = \frac{\sum_{i=1}^{n} \left(d_i - d_i^* \right)}{\sum_{i=1}^{n} L_i}, \tag{5}$$

where d_i^* is the difference given by (3) for the original image, while d_i is that of the given, and possibly, corrupted image. A given image is found to be "noisy" if $\phi > 0$. Likewise, an image is "blurred" if $\phi < 0$.

2.3 Noise and Blur Quantification

In its current form, ϕ is an indirect estimate of the quantity of noise or blurring in a given image. This metric generally assumes large positive values for very noisy images and small, frequently negative, values for those that are severely blurred. The relationship between ϕ and the level of distortion is not, however, a direct one. This means, for instance, that two images, both corrupted by the same amount of random noise, may be assigned different values of ϕ. One of these two images might be highly detailed, while the other may be much less so. Consequently, the value of ϕ depends on the content of the particular image under scrutiny. This is an especially exciting prospect. It essentially means that ϕ is a *perceptual* measure of quality rather than a trivial *mathematical* measure of quality. Other groups find their own names for these types of measures, such as *statistical measures* [5] and *visual front-end models* [5], respectively. In the aforementioned example, the highly detailed image, which conceals noise, appears to be less noisy to a human observer than does the less cluttered image. It is therefore advantageous that the new metric judges them as such. In short, ϕ, as presently computed, is a perceptual estimate of the level of noise or blurring in an image. This is validated using human-derived data in Section 3.2.

3 Experiments and Discussion

As a means of validating the ideas of Section 2, an experiment involving 80 uncorrupted images, each 256×256 in size, was carried out. These images were randomly selected from various sites across the Internet. Six corrupted versions of each of these 80 test images were synthetically generated using random, Gaussian and salt-and-pepper noise, as well as averaging, Gaussian and motion blurring, respectively. In total, $80 \cdot 6 = 480$ corrupted images were created. Together, with the 80 original images themselves, $480 + 80 = 560$ images were tested. Noise was injected in random amounts ranging from 0.01% to 99.99%. The size of the averaging and Gaussian blur *filters* [1] varied between 3×3 and 65×65. As for the motion blur, the direction was randomly chosen between 0° and 359°, with a magnitude of between 1 and 32 pixels in length.

Error	Number of Test Images	Number of Correctly Classified Images	Proportion of Correctly Classified Images
none (error-free)	80	76	95.00%
random noise	80	76	95.00%
Gaussian noise	80	66	82.50%
salt-and-pepper noise	80	79	98.75%
total (noise)	240	221	92.08%
averaging blur	80	79	98.75%
Gaussian blur	80	80	100.00%
motion blur	80	66	82.50%
total (blur)	240	225	93.75%
total	560	522	93.21%

Table 1: Experimental results for no-reference noise, blur and error-free detection using ϕ

3.1 Noise and Blur Detection

Each of the 560 test images was checked for noise, blur or the absence thereof by way of the new metric ϕ of Section 2.2. The actual quantification of the level of noise or blur is explored later in Section 3.2. Beginning first with the detection phase of this experiment, ϕ has proven to be a decidedly very effective metric. This is especially true when it comes to the full-reference case. In this case, only the 480 corrupted images, $80 \cdot 3 = 240$ noisy and $80 \cdot 3 = 240$ blurred, were, of course, analyzed. With the original images in hand, all 240 noisy images were properly marked as being noisy. This represents a classification accuracy of 100%. Likewise, of the 240 blurred images, all 240, or 100%, were labeled as such. This perfect classification is an indication of the strength of the proposed method.

Excellent results were also obtained in the much more challenging no-reference case. Of the 80 original images, 76, or 95.00%, were determined to be free of any errors. These results, along with those of the rest of this section, are organized in Table 1.

Three of these original images are seen in Figure 4. While there are certainly minor differences between the three spectra, given in Figures 4b, 4e and 4h, respectively, the resulting CDFs, shown in Figures 4c, 4f and 4i, respectively, are remarkably similar. The slightly warped shape of the CDF of Figure 4c does not significantly impact the resulting value of ϕ. With a value of -0.1654, ϕ properly falls between the thresholds of T_η and T_β. Of particular interest is the popular "mandrill" image of Figure 4d. Image processing algorithms are frequently confounded by the detailed fur and hair of this image, given that they are quite similar in appearance to noise. In this research, however, there is no confusion between the two phenomena. The image is assigned a score of $\phi = 0.0213$, safely below the cut-off point of $T_\eta = 0.05$.

Take next the 240 noisy images. Each of these images was tested for noise using the threshold $T_\eta = 0.05$. Those corrupted by random noise were correctly identified as being noisy in 76 of the 80 instances, yielding a classification rate of 95.00%. Gaussian noise, perhaps a bit more challenging to detect, was rightly spotted in 66, or 82.50%, of the 80 images corrupted by Gaussian noise. Lastly, salt-and-pepper noise, the most destructive of the three kinds of noise, was picked up in 79 of the 80 images corrupted by that kind of noise, a classification rate of 98.75%. Altogether, of the 240 noisy images, 221 were identified as such. This amounts to an overall

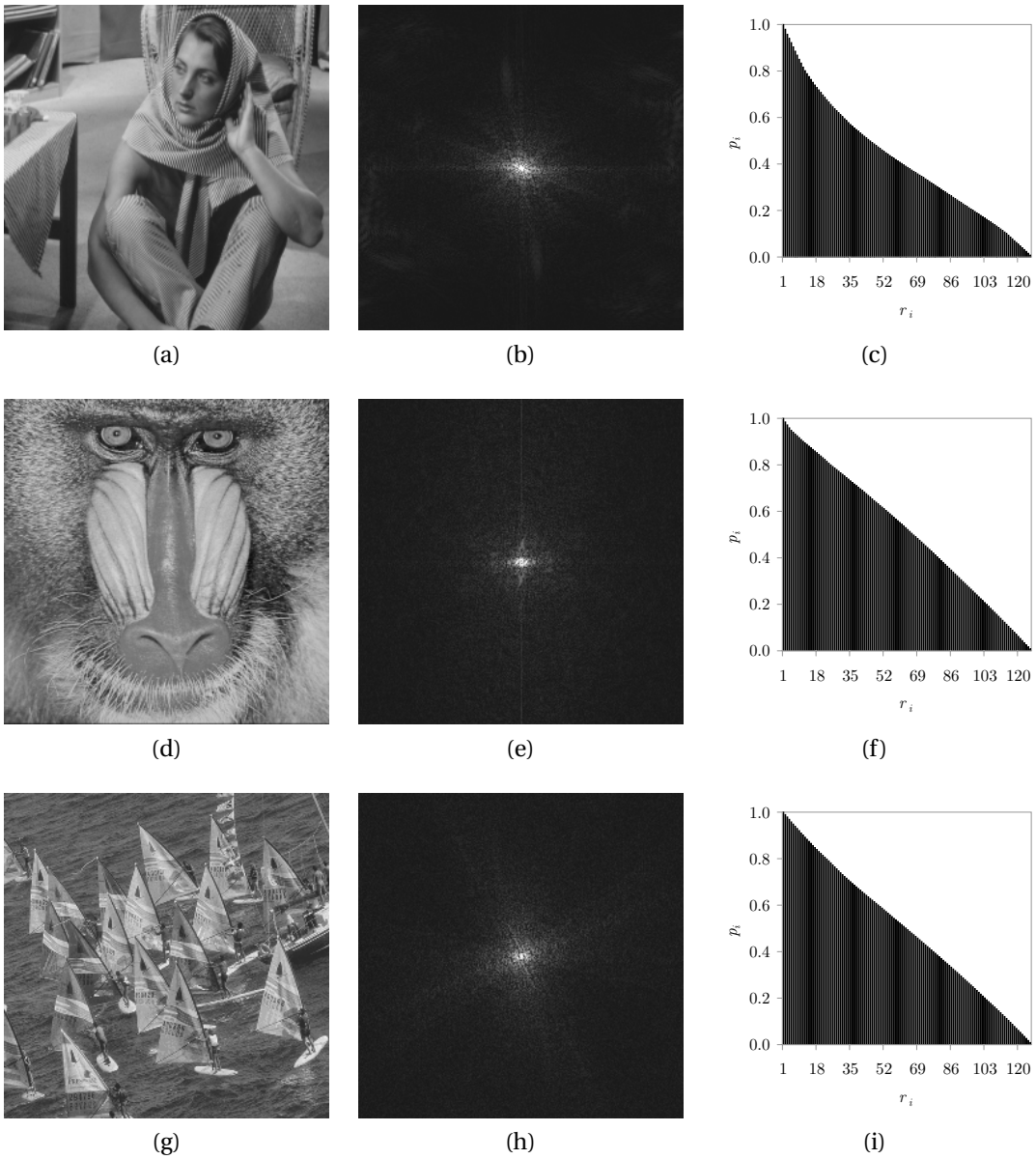

(a) (b) (c)

(d) (e) (f)

(g) (h) (i)

Figure 4: Examples of error-free detection; (a) “Barbara” ($\phi = -0.1654$); (b) “Barbara” spectrum; (c) “Barbara” CDF; (d) “mandrill” ($\phi = 0.0213$); (e) “mandrill” spectrum; (f) “mandrill” CDF; (g) “sails” ($\phi = -0.0032$); (h) “sails” spectrum; (i) “sails” CDF

accuracy rate of 92.08%.

Examples of the noisy images used in this survey are found in Figure 5. The random and salt-and-pepper noise of Figures 5a and 5g, respectively, give rise to pronounced "humps" at the centers of both CDFs, presented in Figures 5c and 5i, respectively. Hence, in both instances, ϕ correctly surpasses the noise threshold T_η. The somewhat inconsequential Gaussian noise of Figure 5d manages to escape detection. When the intensity of this type of noise is particularly low, the accompanying CDF tends to be rather similar to that of an untainted image, as one can deduce from Figure 5f.

Finally, the 240 blurred images were analyzed. Just as in Section 2.2, a blurred image is one in which $\phi < T_\beta = -0.35$. All but one of the 80 images smeared by an averaging filter were properly marked as being blurred. This is therefore an accuracy rate of 98.75%. Perfect classification was observed over all 80 Gaussian-blurred images. Lastly, 66 of the 80 pictures distorted by a motion blur were found to be blurred, producing an accuracy rate of 82.50%. A motion blur tends to preserve more detail than the other two types, making it somewhat more difficult to detect. In total, nevertheless, 225 of the 240 blurred images were correctly found to be blurred, giving an overall accuracy rate of 93.75% for this error.

Three of the blurred images that were tested are seen in the example of Figure 6. Even a minor blur, such as the 3×3 averaging blur of Figure 6a, is caught by the new technique. In this example, ϕ registers a value of -0.5019, below the threshold of $T_\beta = -0.35$. Not surprising, there is also a prominent "dip" in the accompanying CDF of Figure 6c. An even more noticeable "dip" is observed in Figure 6f. This is obviously attributed to the much more destructive 17×17 Gaussian blur of Figure 6d. This distortion ultimately pulls down the value of the new metric, which, in this case, measures in at $\phi = -0.5799$. This value is also below T_β. Lastly, in Figure 6g, a motion blur is applied. This again drives down the value of ϕ, dropping to a value of -0.4860. Once more, this value is below the blurring threshold. As an added remark, note the difference between the spectrum of the image corrupted by the motion blur, given in Figure 6h, and those of the other two types of blurs, given in Figures 6b and 6e. The motion blur, by its very nature, introduces linear-like features that run perpendicular to the direction of the blur. This contrasts with the more arbitrary distribution of points across the spectra of the other two blurred images. In the future, it is hoped that this difference will enable an enhanced ϕ metric to automatically discriminate between a motion blur and an averaging or Gaussian blur. This sort of refined classification would likely prove to be quite challenging when it comes to the three types of noise.

Combining the results of the no-reference case, 522 of the 560 images considered, or 93.21% of them, were properly labeled. These findings underscore the strength of the new metric.

3.2 Noise and Blur Quantification

Having established the ability of the new metric to spot an error, this research next demonstrates its capacity to measure the perceived intensity of an error. This was done using the human user study first presented in [7, 8]. In this study, randomly chosen participants were asked to assess the perceived quality of a series of corrupted images. Fourteen "classic" images, some of which have already been encountered in this paper, were selected for this study. All of these may be seen in [7, 8]. Each of these 14 images was artificially corrupted by one of noise, blurring or *compression* [1]. This procedure was repeated five times, thereby producing

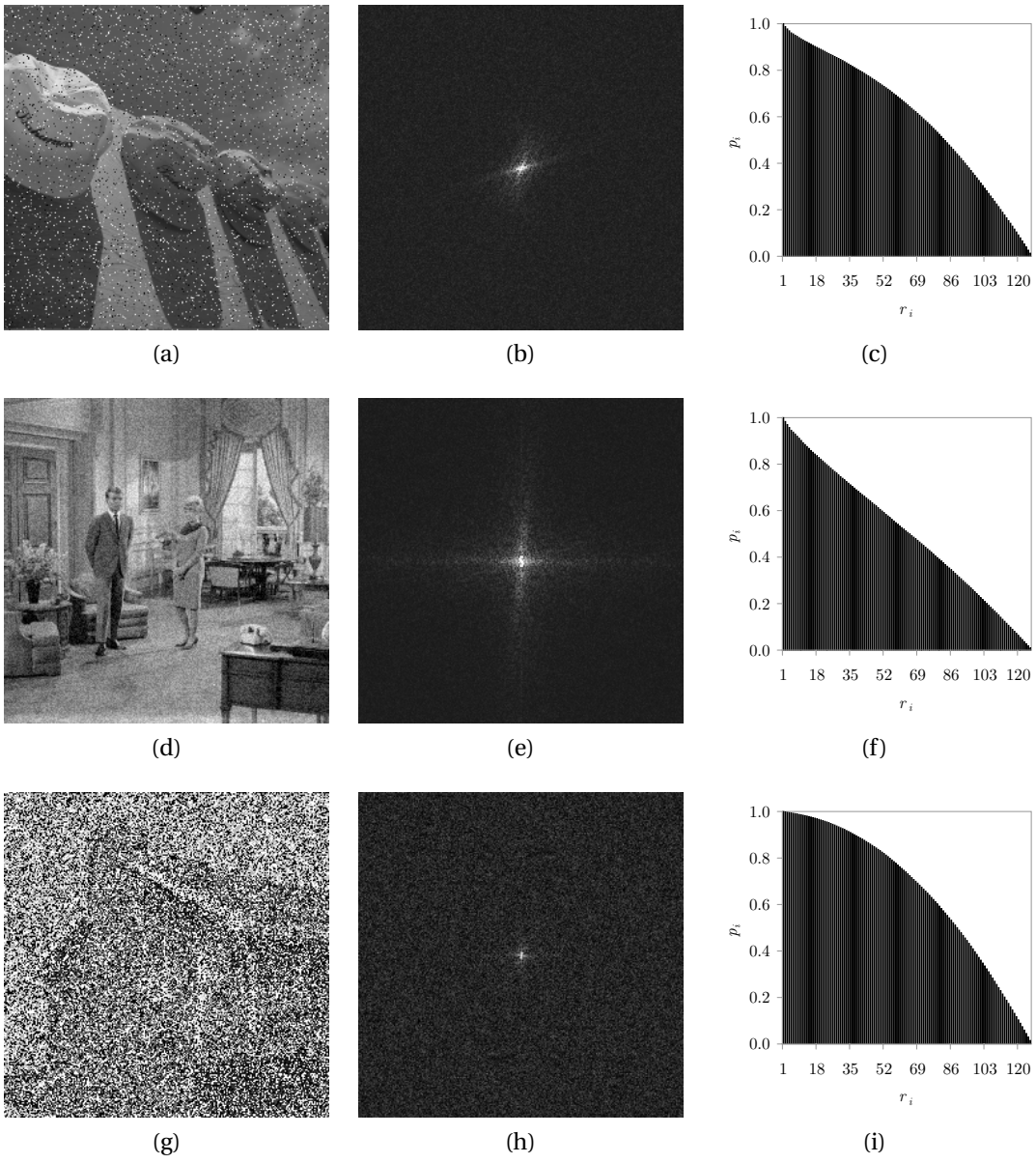

Figure 5: Examples of noise detection; (a) “hats” (7.33% random noise), ($\phi = 0.2016$); (b) “hats” (7.33% random noise) spectrum; (c) “hats” (7.33% random noise) CDF; (d) “couple” (10.11% Gaussian noise), ($\phi = 0.0060$); (e) “couple” (10.11% Gaussian noise) spectrum; (f) “couple” (10.11% Gaussian noise) CDF; (g) “house” (58.31% salt-and-pepper noise), ($\phi = 0.3139$); (h) “house” (58.31% salt-and-pepper noise) spectrum; (i) “house” (58.31% salt-and-pepper noise) CDF

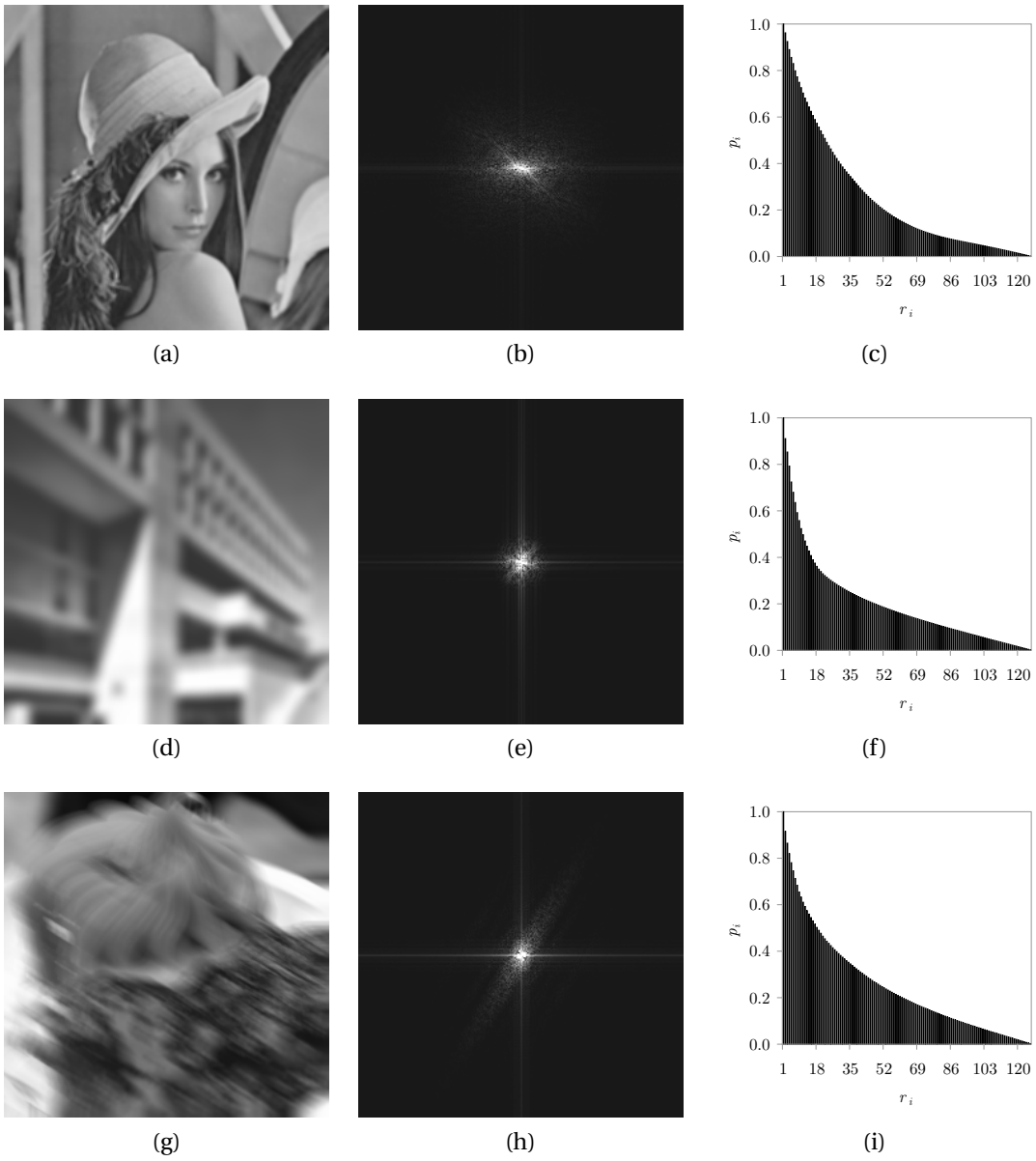

Figure 6: Examples of blur detection; (a) “Lena” (3×3 averaging blur), ($\phi=-0.5019$); (b) “Lena” (3×3 averaging blur) spectrum; (c) “Lena” (3×3 averaging blur) CDF; (d) “MIT” (17×17 Gaussian blur), ($\phi=-0.5799$); (e) “MIT” (17×17 Gaussian blur) spectrum; (f) “MIT” (17×17 Gaussian blur) CDF; (g) “dessert” (32°, 21-magnitude motion blur), ($\phi=-0.4860$); (h) “dessert” (32°, 21-magnitude motion blur) spectrum; (i) “dessert” (32°, 21-magnitude motion blur) CDF

Error	Number of Test Images	Number of Correctly Classified Images	Proportion of Correctly Classified Images
none (error-free)	13	13	100.00%
random noise	9	8	88.89%
Gaussian noise	7	4	57.14%
salt-and-pepper noise	5	5	100.0%
total (noise)	21	17	80.95%
averaging blur	10	10	100.00%
Gaussian blur	7	6	85.71%
motion blur	4	4	100.00%
total (blur)	21	20	95.24%
total	55	50	90.91%

Table 2: Experimental results for no-reference noise, blur and error-free detection using ϕ (human user study)

five corrupted versions of each of the 14 images. Thus, in total, $14 \cdot 5 = 70$ corrupted images were generated. Those tainted by compression errors are not discussed in this paper as they are not relevant, thereby leaving only $70 - 15 = 55$ images to consider. Each of the human participants in this experiment was shown one of the five damaged images, arbitrarily selected, from each of the 14 "sets" of corrupted images. They were asked to identify the quality of each image as being either "unusable", "poor", "fair", "good" or "excellent", using the numerical values 0, 1, 2, 3 and 4, respectively. These numerical scores were subsequently averaged over all 73 participants, resulting in individual *mean opinion scores* [30] (MOS) for each of the 55 corrupted images. Lastly, by way of the *Pearson product-moment correlation coefficient* [31], the mean opinion scores were compared with the individual ϕ scores assigned to each of these 55 test images. In the case of those impaired by noise, the level of correlation comes in at $\rho = -0.6856$, with an associated *student t* [24] statistic of $t^* = -4.1048$. As for the blurred images, the correlation stands at $\rho = 0.6456$, with $t^* = 3.6850$. These results attest to the genuine difficulties encountered when attempting to perceptually quantify errors. In this research, however, this is of much lesser concern given that the focus is that of the detection, rather than the perceptual quantification, of errors. And, as the evidence of Table 2 shows, this research is again successful when it comes to the issue of detecting errors. Overall, a 90.91% accuracy in classification is achieved, a value that follows just behind the strong result obtained earlier in Section 3.1.

4 Conclusion

When organized into a cumulative distribution function, frequency information allows for easy and reliable classification of images. In particular, those that are noisy, blurred or otherwise uncorrupted may be individually separated from one another using a new metric. The exact degree of noise or blur depends on the content of the specific image in question. Future directions include refining the thresholds employed in this work, as well as distinguishing between the individual types of blurring and, perhaps, noise. Color is another tempting prospect, given that color images offer more information than do grayscale images. This could ultimately lead

to even better performance when it comes to error detection. Lastly, and perhaps most significant of all, is the task of verifying the implied conjecture that an uncorrupted image generally produces a more or less balanced CDF. At the moment, this issue has only been addressed from an empirical perspective. A more formal examination of this idea is needed.

5 Acknowledgements

This research was funded by a grant from the Natural Sciences and Engineering Research Council of Canada (NSERC). Further thanks are extended to the University of Regina Research Ethics Board (REB) for their efforts in approving the human user study described in this work.

References

[1] Rafael Gonzalez and Richard Woods. *Digital Image Processing*. Prentice Hall, 2002.

[2] Milan Sonka, Vaclav Hlavac, and Roger Boyle. *Image Processing, Analysis and Machine Vision*. Brooks/Cole, 1999.

[3] Stuart Perry, Hau San Wong, and Ling Guan. *Adaptive Image Processing: A Computational Intelligence Perspective*. CRC Press, 2002.

[4] Lynn Loomis. *Calculus*. Addison-Wesley, 1974.

[5] Ruud Janssen. *Computational Image Quality*. SPIE Press, 2001.

[6] Sabine Süsstrunk and Stefan Winkler. Color image quality on the internet. *Proc. IS&T/SPIE Electronic Imaging 2004 Conf: Internet Imaging V*, 5304:118–131, December 2003.

[7] Richard Dosselmann and Xue Dong Yang. No-reference image quality assessment using level-of-detail. Technical Report CS 2011-2, University of Regina, Regina, Saskatchewan, Canada, May 2011.

[8] Richard Dosselmann. *Image Quality Assessment using Level-of-Detail*. PhD thesis, University of Regina, 2012.

[9] Shahriar Kaisar, Sakib Rijwan, Jubayer Al Mahmud, and Muhammad Rahman. Salt and pepper noise detection and removal by tolerance based selective arithmetic mean filtering technique for image restoration. *Int. Journal Computer Science and Network Security*, 8(6):271–278, June 2008.

[10] Jafar Mohammed. An improved median filter based on efficient noise detection for high quality image restoration. *Second Asia Int. Conf. Modeling & Simulation*, pages 327–331, May 2008.

[11] Takanori Sato, Noritaka Yamashita, Yoshinori Ito, Jianming Lu, Hiroo Sekiya, and Takashi Yahagi. Impulse noise detector using absolute deviation and spatial relations between the color components for color images. *2006 RISP Int. Workshop Nonlinear Circuit and Signal Processing*, pages 279–282, March 2006.

[12] Marc Hensel, Gordon Wiesner, Bernd Kuhrmann, Thomas Pralow, and Rolf-Rainer Grigat. Motion and noise detection for adaptive spatio-temporal filtering of medical X-ray image sequences. *14th Int. Conf. Medical Physics*, 50:219–222, 2005.

[13] Bogdan Smolka. Adaptive impulsive noise removal in color images. *Proc. Asia-Pacific Signal and Information Processing Association Annual Summit and Conf.*, pages 755–764, October 2009.

[14] Jaakko Astola, Petri Haavisto, and Yrjö Neuvo. Vector median filters. *Proc. IEEE*, 78(4), April 1990.

[15] George Luger. *Artificial Intelligence: Structures and Strategies for Complex Problem Solving*. Pearson, 6th edition, 2009.

[16] V. Saradhadevi and V. Sundaram. A novel two-stage impulse noise removal technique based on neural networks and fuzzy decision. *Int. Journal Computer Applications*, pages 31–42, 2011.

[17] Richard Duda, Peter Hart, and David Stork. *Pattern Classification*. John Wiley & Sons, 2001.

[18] Zhou Wang and David Zhang. Impulse noise detection and removal using fuzzy techniques. *IEE Electronics Letters*, 33(5):378–379, February 1997.

[19] Li-Xin Wang. *A Course in Fuzzy Systems and Control*. Prentice Hall PTR, 1997.

[20] Pina Marziliano, Frederic Dufaux, Stefan Winkler, and Touradj Ebrahimi. Perceptual blur and ringing metrics: Application to JPEG2000. *Signal Processing: Image Communication*, 19(2):163–172, 2004.

[21] Yun-Chung Chung, Jung-Ming Wang, Robert Bailey, Sei-Wang Chen, and Shyang-Lih Chang. A non-parametric blur measure based on edge analysis for image processing applications. *Proc. IEEE Conf. Cybernetics and Intelligent Systems*, 1:356–360, 2004.

[22] Gang Cao, Yao Zhao, and Rongrong Ni. Edge-based blur metric for tamper detection. *Journal Information Hiding and Multimedia Signal Processing*, 1(1):20–27, January 2010.

[23] Anat Levin. Blind motion deblurring using image statistics. *Advances in Neural Information Processing Systems*, December 2006.

[24] Donald Sanders and Robert Smidt. *Statistics: A First Course*. McGraw-Hill, 2000.

[25] D. Tolhurst, Y. Tadmore, and Tang Chao. Amplitude spectra of natural images. *Ophthalmic and Physiological Optics*, 12(2):229–232, April 1992.

[26] Renting Liu, Zhaorong Li, and Jiaya Jia. Image partial blur detection and classification. *IEEE Conf. Computer Vision and Pattern Recognition*, pages 1–8, 2008.

[27] Ming-Jun Chen and Alan Bovik. No-reference image blur assessment using multiscale gradient. *Int. Workshop Quality of Multimedia Experience*, pages 70–74, 2009.

[28] Abe Shigeo. *Support Vector Machines for Pattern Classification.* Springer, 2005.

[29] William Hays and Robert Winkler. *Statistics: Probability, Inference, and Decision.* Holt, Rinehart and Winston, 1971.

[30] Stefan Winkler. *Digital Video Quality: Vision Models and Metrics.* John Wiley & Sons, 2005.

[31] John Neter, Michael Kutner, Christopher Nachtsheim, and William Wasserman. *Applied Linear Statistical Models.* Irwin, 1996.